

Impact of the occupancy scenario on the hygrothermal performance of a room

Rudy Bui, Matthieu Labat, Sylvie Lorente

▶ **To cite this version:**

Rudy Bui, Matthieu Labat, Sylvie Lorente. Impact of the occupancy scenario on the hygrothermal performance of a room. Building and Environment, 2019, 160, pp.106178. 10.1016/j.buildenv.2019.106178 . hal-02165644

HAL Id: hal-02165644

https://hal.insa-toulouse.fr/hal-02165644

Submitted on 26 Jun 2019

HAL is a multi-disciplinary open access archive for the deposit and dissemination of scientific research documents, whether they are published or not. The documents may come from teaching and research institutions in France or abroad, or from public or private research centers.

L'archive ouverte pluridisciplinaire **HAL**, est destinée au dépôt et à la diffusion de documents scientifiques de niveau recherche, publiés ou non, émanant des établissements d'enseignement et de recherche français ou étrangers, des laboratoires publics ou privés.

Impact of the occupancy scenario on the hygrothermal performance of a room

Rudy Bui, Matthieu Labat*, Sylvie Lorente

May 30, 2019

LMDC, Université de Toulouse, UPS, INSA, France

* corresponding author at LMDC, INSA/UPS Génie Civil, 135 Avenue de Rangueil, 31077 Toulouse cedex 04 France.

E-mail address: m_labat@insa-toulouse.fr

Abstract

Nowadays, humidity in buildings has become a major concern because it affects their energy performance, the occupants' comfort and health, and the durability of materials simultaneously. To understand the behavior of buildings towards humidity, numerical models are needed. However, the sensitivity of these models to the indoor sources, especially the ones related to the occupants' presence and activities, has not been thoroughly assessed in the literature. This article proposes to introduce a methodology to investigate the impact of the occupancy profiles of presence on the hygrothermal performance of a room. A hygrothermal model at room scale is developed and coupled with a platform called No-MASS, which provides stochastic occupancy scenarios for office buildings. Four occupancy scenarios representative of the scenarios commonly found in the literature are studied: a stochastic scenario, an average scenario derived from multiple stochastic ones, a constant scenario, and

the French regulatory scenario. Comparing the results obtained with the different occupancy scenarios underlined a non-negligible impact of the scenario on indoor heat and moisture balance, mainly due to the consideration of a seasonal effect for the stochastic one.

Keywords heat and mass transfer; occupants' presence modelling; hygrothermal performance; numerical modelling

Nomenclature

Greek letters

δ	Permeability (s)
ϵ	Emissivity
κ	Absorptivity
Ψ	Relative humidity
ρ	Density (kg/m^3)
σ	Stefan-Boltzmann constant $(W/(m^2.K^4))$

Latin letters

$\dot{m}$	Vapor flux (kg/s)
$\dot{Q}$	Heat flux (W)
A	Surface (m^2)
a, c	Empirical parameters
C_p	Heat capacity $(J/(kg.K))$
dt	Time step (s)
g	Mass flux density $(kg/(m^2.s))$
h	Convective transfer coefficient $(kg/(m^2.s.Pa))$ or $(W/(m^2.K))$
k	Thermal conductivity $(W/(m.K))$
L	Latent heat (J/kg)

n	Ventilation rate (s^{-1})
p	Pressure (Pa)
q	Heat flux density (W/m^2)
R	Ideal gas constant ($J/(kg.K)$)
S	Source term (kg/s) or (W)
T	Temperature (K)
t	Time (s)
V	Volume (m^3)
w	Water content (kg/m^3)
x	Mass ratio

Subscripts

a	Air
AC	Air-conditioner
atm	Atmosphere
c	Capillary
$conv$	Convective
$crit$	Critical
$dehumid$	Dehumidifier
ext	Exterior
$humid$	Humidifier
int	Interior
sat	Saturation
v	Vapor
$ventil$	Ventilation

1 Introduction

With the growing energy consumption of buildings, strategies to save energy have become a priority. Consequently, building insulation is constantly improving, leading to airtight constructions. However, this also raises new challenges, especially issues related to humidity in buildings as it has a simultaneous impact on the energy consumption, the occupants' comfort and health, and the durability of materials. The main phenomena influencing indoor humidity balance are the moisture interactions between indoor air and walls, the ventilation and the indoor moisture sources [1]. To investigate these issues, numerical hygrothermal models are needed. Many models already exist in the literature; MATCH [2] and WUFI [3] can be mentioned among others. Refs. [4] and [5] are referred to as reviews on hygrothermal models.

What differs greatly from one hygrothermal model at room scale to another is the description of indoor sources, especially those related to the occupants' presence and activities. The simplest approach is to assume that the occupants generate a constant amount of water vapor throughout the day due to their presence and activities. This is exemplified in Ref. [6], in which a constant production of 7.7 kg/day plus $1kg/day$ on wash day was selected. In Ref. [7], it was shown that a constant production rate of 270 g/h was representative of a family of four based on the review of 9 studies in the literature.

Another widespread approach is to assume a deterministic scenario, meaning that the occupants are present every day at fixed times. It is worth noting that the French regulation RT 2012 [8] governing the construction of new buildings uses deterministic occupancy scenarios to size the air-conditioning system. In Ref. [9], the moisture production rate due to the occupants' presence was 3 $g/m^3/h$ during occupied periods and 0.5 $g/m^3/h$ during unoccupied periods. This study aims to develop a whole-building hygrothermal model by considering the occupants' presence and to propose an estimation of the effect of walls moisture buffering on the occupants' comfort and the energy consumption. In Ref. [10], a production rate of

0.5 $g/m^3/h$ was selected with peaks in the morning and in the evening at 8 $g/m^3/h$ am and 4 $g/m^3/h$ respectively. Among hygrothermal studies using a deterministic occupancy scenario, Refs. [11] and [12] are worthy of attention.

While deterministic scenarios are easy to implement, they do not mirror the occupants' real behavior in buildings. Therefore, stochastic models might be an interesting alternative. Rather than defining fixed presence times, such models consider probabilities of presence. This is an emerging approach in the field of energy performance. For example, in Ref. [13], a stochastic model of presence based on inhomogeneous Markov chains was developed. It was then calibrated with data obtained by monitoring a university building for 5 years. This model and numerous activity models, were successfully employed in Ref. [14] to quantify the influence of the occupants on a building energy performance based on a sensitivity analysis. In Ref. [15], a wide range of activities were modelled. The activities having the most impact on the energy performance of a building were extracted from Time Use Survey (TUS) data. The occupants' interactions with windows and blinds were modelled in Refs. [16] and [17] on the basis of their real behavior in an office building. The validation was based on the monitoring of a building for 7 years. The Lightswitch-2002 model [18] was developed to predict the use of lighting by occupants. Additionally, a platform combining presence and activity modelling for offices and residential houses was proposed in Ref. [19], where a comparison with a deterministic scenario was also provided to quantify the difference in heating and cooling demand. This work demonstrated that a deterministic scenario could lead to an underestimation of 20% in heating and cooling demand. These examples point out that models of occupants' presence and activities are still undergoing development in the field of energy performance. A more complete state of the art on the stochastic functionality of several models can be found in Ref. [20].

To date, few hygrothermal model include the stochastic nature of the occupants' behavior. The state of the art presented in Ref. [21] shows that among 9 hy-

grothermal models, none took it into consideration. Recently, Ref. [22] introduced a methodology to estimate the moisture buffering effect of walls subjected to realistic conditions depicted by the stochastic modelling of the occupants' presence and activities. Labat and Woloszyn's stochastic modelling [21] was based on a TUS carried out in Belgium. They selected a profile corresponding to a student or a young working individual. A comparison between a stochastic and a constant occupancy scenario highlighted an underestimation of 50 to 80% of the flux exchanged between the air and the walls when a constant moisture rate was applied. In this study, only an ideal heating system with a set point temperature of 20°C was modelled. Finally, Winkler et al. [23] modelled the occupants' behavior in a stochastic way and took into consideration the vapor production due to their presence and activities. The variations in internal loads related to the occupants significantly impacted the indoor humidity. Also, it was showed that the moisture buffering effect of the walls had a limited impact on the indoor humidity compared to the regulation of the air-conditioning system.

This short literature review shows that the use of stochastic occupancy scenarios in hygrothermal models is not common, but a few examples have been proposed recently. To investigate the relevance of using stochastic scenarios in hygrothermal modelling, this paper proposes an estimation of the impact of the occupancy scenario on indoor heat and moisture balances. A numerical methodology is presented that takes the heat and moisture exchange with the walls into account as well as the indoor sources represented by an air-conditioning system and the occupants' presence and activities. A study of the occupancy scenario was conducted to quantify its impact on performance indicators: the energy consumption of the air-conditioning equipment, the indoor hygric comfort and moisture-related risks concerning the walls.

Firstly, the whole methodology applied to a specific case study is presented in

Section 2. The coupled heat and moisture transfer model at wall scale is described in Section 3, followed by the indoor sources in Section 4. The performance indicators used to quantify the hygrothermal performance of a room are defined in Section 5. Finally, different occupancy scenarios are modelled (Section 6) and their impact on the performance indicators is assessed in Section 7.

2 Methodology

The hygrothermal performance of a room is strongly dependent on the indoor air ambient conditions (temperature and relative humidity). The factors influencing these conditions are the heat and moisture exchange with the walls and the indoor sources. This is illustrated by Fig. 1.

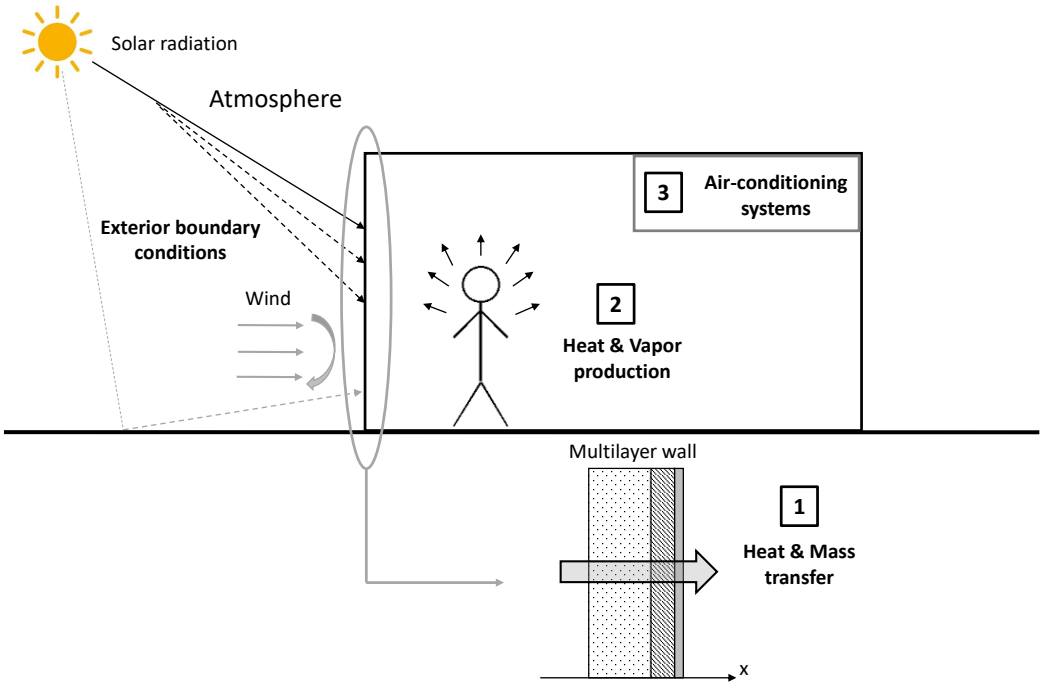


Figure 1: Schematic representation of the different modelling elements

In buildings, heat and moisture sources ($\dot{Q}_{int}$ and $\dot{m}_{int}$) are determined by the occupants' presence and activities and by the use of air-conditioning equipment. Therefore, modelling these different parts is a necessity in order to propose an esti-

mation of the energy consumption and the comfort conditions of a room. The first step towards this goal is to write the mass and energy balance equations for indoor air. The mass conservation equation at the room scale is given by Eq. (1):

$$\frac{R_a}{R_v} \cdot \frac{\rho_a V p_{atm}}{(p_{atm} - p_{v,int})^2} \frac{\partial p_{v,int}}{\partial t} = \sum_i \dot{m}_i = \dot{m}_{walls} + \dot{m}_{ventil} + \dot{m}_{int} \tag{1}$$

where R_a is the specific gas constant of air $(J/(kg.K))$, R_v is the specific gas constant of water vapor $(J/(kg.K))$, ρ is the density (kg/m^3), V is the volume of the room (m^3), p_{atm} is the atmospheric pressure (Pa), p_v is the water vapor pressure (Pa), t is the time (s), subscripts a, v and int stand for *air*, *vapor* and *interior* respectively, $\dot{m}_{walls}$ is the convective water vapor exchange with the walls (kg/s), $\dot{m}_{ventil}$ is the vapor exchange with the exterior environment due to the ventilation (kg/s) and $\dot{m}_{int}$ is the indoor vapor source/sink term (kg/s). The development of the right hand side of Eq. (1) is given by Eq. (2):

$$\begin{aligned} \dot{m}_{walls} &= \sum_j A_j h_{m,int} (p_{v,is,j} - p_{v,int}) \\ \dot{m}_{ventil} &= \frac{R_a}{R_v} \cdot \rho_a n V \left(\frac{p_{v,ext}}{p_{atm} - p_{v,ext}} - \frac{p_{v,int}}{p_{atm} - p_{v,int}} \right) \end{aligned} \tag{2}$$

where A_j is the surface of the wall j (m^2), h_m is the convective mass transfer coefficient $(kg/(m^2.s.Pa))$, n is the air change rate due to the ventilation (s^{-1}) and subscripts *is* and *ext* stand for *interior surface* and *exterior* respectively.

Eq. (3) also gives the energy balance, similarly to the mass balance equation, but includes the latent heat contribution:

$$\begin{aligned} &\rho_a V (c_{p,a} + \frac{R_a}{R_v} \cdot \frac{p_{v,int}}{p_{atm} - p_{v,int}} c_{p,v}) \frac{\partial T_{int}}{\partial t} \\ &= \dot{Q}_{walls} + \dot{Q}_{ventil} + \dot{Q}_{int} + (c_{p,v} T + L_v) \sum_i \dot{m}_i \end{aligned} \tag{3}$$

where c_p is the heat capacity $(J/(kg.K))$, T is the temperature (K) $\dot{Q}_{walls}$ is the

convective heat exchange with the walls (W), $\dot{Q}_{ventil}$ is the heat exchange with the exterior environment due to the ventilation (W), $\dot{Q}_{int}$ is the indoor heat source/sink term (W) and L_v is the latent heat of vaporization (J/kg). Eq. (4) details the right hand side of Eq. (3):

$$\begin{aligned} \dot{Q}_{walls} &= \sum_j A_j h_{h,int}(T_{is,j} - T_{int}) \\ \dot{Q}_{ventil} &= nV\rho_a c_{p,a}(T_{ext} - T_{int}) \end{aligned} \tag{4}$$

The exchanges between the indoor air and the walls, characterized by $\dot{m}_{walls}$ and $\dot{Q}_{walls}$, depend on the hygrothermal transfer through the walls. Hence, the coupled heat and moisture transfer at wall scale has to be studied first.

3 Coupled heat and moisture transfer in the walls

3.1 Governing equations

Transfer in porous materials is governed by mass and energy conservation equations. The governing equations used in this work are taken from Refs. [24] and [25], and are written for a one-dimensional case. They are briefly presented in this section; the full demonstration can be found in Ref. [24].

Mass conservation accounts for water vapor and liquid water transport described by Fick's and Darcy's laws respectively (Eq. (5)):

$$\frac{\partial w}{\partial t} = -\frac{\partial}{\partial x}\left(\delta_l \frac{\partial p_c}{\partial x} - \delta_v \frac{\partial p_v}{\partial x}\right) \tag{5}$$

where w is the water content of the material (kg/m^3), δ_l is the liquid water permeability (s), p_c is the capillary pressure (Pa) and δ_v is the water vapor permeability (s).

While heat transfer is driven by the temperature, different driving potentials may

be used for the moisture transport. According to a literature review (not presented here), models using the capillary pressure perform better — regarding accuracy and numerical performance — than the ones using other driving potentials such as the water content [26], the vapour pressure [27], the relative humidity [3] or the logarithm of the capillary pressure [28]. Hence, it was chosen as the mass driving potential. Consequently, after some mathematics Eq. (5) becomes:

$$\frac{\partial w}{\partial p_c} \cdot \frac{\partial p_c}{\partial t} = -\frac{\partial}{\partial x}\left[\left(\delta_l + \delta_v \frac{\rho_v}{\rho_l}\right)\frac{\partial p_c}{\partial x} - \delta_v \left(\Psi \frac{\partial p_{v,sat}}{\partial T} - p_v \frac{ln\Psi}{T}\right)\frac{\partial T}{\partial x}\right] \tag{6}$$

where ρ_l is the liquid water density (kg/m^3) and Ψ is the relative humidity ($-$).

The first law of thermodynamics states that the rate of energy accumulated within a control volume is equal to the net heat transfer of energy by conduction plus the net transfer of energy by fluid flow [29]. It is given by Eq. (7):

$$\left(\rho_s c_s + \sum_i w_i c_{p,i}\right)\frac{\partial T}{\partial t} = k_{mat}\frac{\partial^2 T}{\partial x^2} - \sum_i w_i \nu_i c_{p,i}\frac{\partial T}{\partial x} - [(c_{p,l} - c_{p,v})T - L_v]S_l \tag{7}$$

where k_{mat} is the thermal conductivity ($W/(m.K)$) of the material and $w_i\nu_i$ is the mass flow rate per surface unit of the component i.

The source term S_l is calculated thanks to the liquid and solid water conservation equations:

$$\left(\frac{1}{1-\rho_v/\rho_l}\right)\frac{\partial w}{\partial p_c} \cdot \frac{\partial p_c}{\partial t} = -\frac{\partial}{\partial x}\left(\delta_l \frac{\partial p_c}{\partial x}\right) + S_l \tag{8}$$

Finally, the coupled heat and moisture transfer model is characterized by Eqs. (6), (7) and (8). This coupled non-linear model was solved with a finite difference method for a multilayer wall. An implicit scheme was chosen, based on Refs. [30] and [31]. This model was computed in PYTHON [32] with a non-uniform spatial discretisation, meaning that the mesh size was refined at the interfaces between the wall assemblies, as well as between the wall and the air.

An adaptive time stepping method was used for the temporal discretisation [33].

3.2 Validation test

The coupled heat and moisture transfer module validation was based on the standard provided in Ref. [34]. A semi-infinite wall initially at $T = 20°C$ and $\Psi = 50\%$ was subjected to Dirichlet boundary conditions, $T = 30°C$ and $\Psi = 95\%$, applied on its left surface. The wall was made of one material, the properties of which - corresponding to a load-bearing material - are specified in the standard. To satisfy this standard, the water content and temperature profiles at different time, namely 7, 30 and 365 days, must be within $\pm$ 2.5% of an analytical solution. The semi-infinite wall was simulated by adopting a 20 m thickness. While the left surface was subjected to Dirichlet boundary conditions, the fluxes were set null for the surface at the opposite end of the wall, meaning the right surface. This thickness led to a negligible 0.2°C increase of temperature on the right surface. In any case, the water content evolution was limited to the first 20 cm. The profiles are plotted on Fig. 2 where the $\pm$2.5% intervals are represented by the dots.

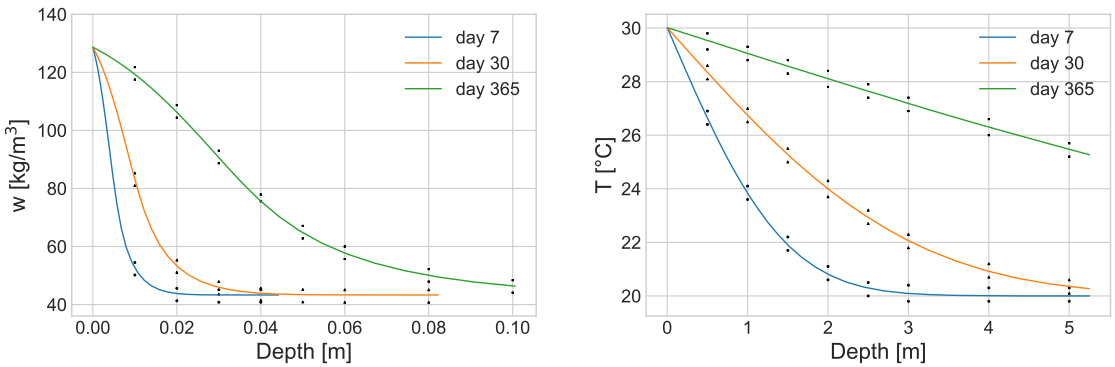


Figure 2: Water content (left) and temperature (right) profiles at 7, 30 and 365 days

All of the profiles presented Fig. 2 are within $\pm$2.5% of the analytical solution, meaning that the model was in conformity with the standard. Additionally, the maximum difference between the calculated profiles and the standard was $0.83 kg/m^3$ for the water content and 0.05°C for the temperature, leading to a satisfactory accuracy.

The simulations were carried out with a non-uniform mesh grid (refined at the

interfaces). This grid was defined by the size of the first mesh, set arbitrarily at $5 \cdot 10^{-4} m$, and a progressive factor characterizing the size of the adjacent meshes. Different progressive factor — leading to a different number of meshes — were tested, namely 1.30, 1.20, 1.15, 1.10 and 1.05. A progressive factor of 1.20 and higher did not allow the model to pass the standard, and it barely passes it with a factor of 1.15. The calculation time was $54.08 \pm 2.01\ s$ for a factor of 1.10, which was deemed reasonable. A factor of 1.05 approximately doubled the calculation time compared to 1.10 for a negligible gain in accuracy on the temperature and water content profiles. Therefore, a progressive factor of 1.10 was selected as it gave the best compromise between the model accuracy and the calculation time.

3.3 Exterior boundary conditions

The exterior boundary conditions were taken from RT 2012 [8] which governs new building construction in France.

Both exterior and interior boundary conditions accounted for the convective heat and mass transfer with the air, given respectively by $q_{h,conv}$ and g_{conv}:

$$q_{h,conv} = h_{h,ext}(T_{ext} - T_{es}) \tag{9}$$

$$g_{conv} = h_{m,ext}(p_{v,ext} - p_{v,es}) \tag{10}$$

where $h_{h,ext}$ is the exterior convective heat transfer coefficient (CHTC, in $W/(m^2.K)$), $h_{m,ext}$ is the convective mass transfer coefficient (CMTC, in $kg/(m^2.s.Pa)$) and subscript es stand for *exterior surface*. Note that these same equations were used for the convective exchange with the indoor air.

The convective mass transfer is a function of the vapor pressure (Eq. (10)). To make it compatible with the coupled heat and mass transfer model at wall scale, it must be written as a function of the capillary pressure. The relative humidity is

related to the capillary pressure through the Gibbs equation for the energy of the interface between the liquid and vapor phases (Eq. (11)):

$$g_{conv} = h_{m,ext}\left[p_{v,ext} - p_{sat}(T_{es})exp\left(-\frac{p_{c,es}}{\rho_l R_v T_{es}}\right)\right] \tag{11}$$

where p_{sat} is the saturated water vapor pressure (Pa). Note that the model written at wall scale uses the capillary pressure as the driving potential, which is suitable for a porous medium but not for a gaseous volume.

The CMTC was calculated thanks to the Lewis analogy (quoted by Ref. [35]):

$$h_{m,ext} = 7.7 \times 10^{-9} \cdot h_{h,ext} \tag{12}$$

The latent contribution due to the vapor exchange was also added and is given by Eq. (13):

$$q_{m,conv} = (c_{p,v}T_{es} + L_v)g_{conv} \tag{13}$$

For the exterior boundary conditions, the impact of the solar radiation was taken into account. It is the sum of long wave-radiation (with the ground and the sky) q_{LWR} and short-wave radiation (direct Dir, diffuse Dif and reflected Ref solar radiation) q_{SWR}:

$$q_{LWR} = \sigma\epsilon F_{gro}(T_{gro}^4 - T_{es}^4) + \sigma\epsilon F_{sky}(T_{sky}^4 - T_{es}^4) \tag{14}$$

$$q_{SWR} = \kappa(Dir + Dif + Ref) \tag{15}$$

where σ is the Stefan-Boltzmann constant ($W/(m^2.K^4)$), ϵ is the emissivity, F_{gro} and F_{sky} are the ground and sky view factors respectively, each taken to be equal to 0.5, and κ is the absorptivity of the wall surface material.

4 Indoor sources

As introduced in Section 2, the indoor heat and water vapor sources are assumed to be the air-conditioning equipment and the occupants' presence and activities in buildings.

The air-conditioning system can be decomposed into a ventilation system, a heater, a humidifier and an air-conditioner and are presented in Section 4.1.

Section 4.2 presents how the occupants' presence and activities were modelled in a stochastic way.

4.1 Air-conditioning system

The ventilation rate was considered as fixed and equal to 25 m^3/h per occupant as this corresponds to the minimum hygienic rate requirement indicated in the French labour law [36]. The ventilation system was supposed to be always turned on.

For heating purposes, a heater was designed to provide a constant heating power Q_{heat} (W). Daytime and nigh-time set point temperatures were selected, with a hysteresis of 0.5°C. Fig. 3 illustrates the regulation of the temperature in a room for set point temperatures equal to 19°C for the night and 21°C for the day. The thermostat switched to the day temperature one hour before the arrival of an occupant in the room, and to the night temperature one hour before his departure to take advantage of the room inertia.

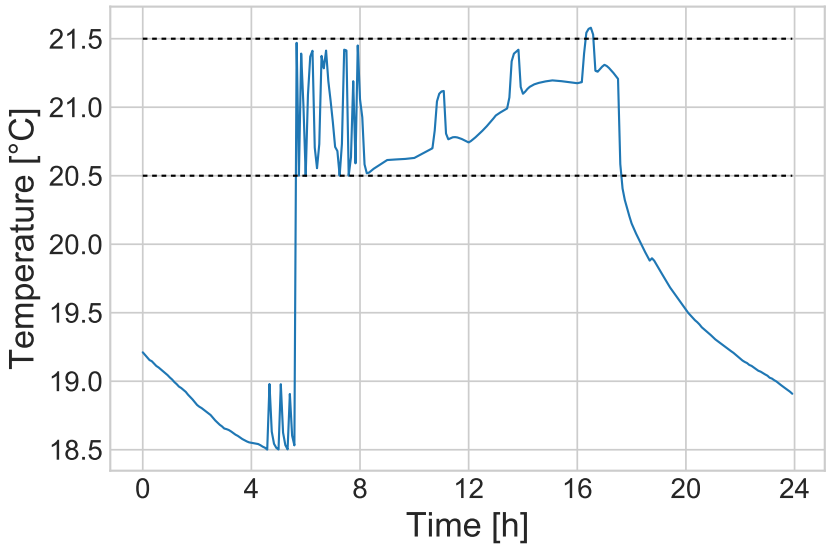


Figure 3: Regulation of the temperature in the course of a day with a hysteresis of 0.5°C

The humidifier also provided constant water vapor $\dot{m}_{humid}$ (kg/s). Its hysteresis was 2%. The humidifier was only turned on during working hours.

For air cooling, a split-type air-conditioner was modelled under the assumption that the rate of the split $\dot{m}_{AC}$ was constant, and the temperature of the refrigerant fluid was equal to 2 °C. Similarly to the heater, it had a hysteresis of 0.5°C. The air-conditioner was turned on only during working hours. The air dehumidification was a consequence of cooling it, since the split type air-conditioner also removed water vapor. The dehumidification rate $\dot{m}_{dehumid}$ was calculated as follows:

$$\dot{m}_{dehumid} = \dot{m}_{AC}(x_{AC} - x_{int}) \tag{16}$$

where $\dot{m}_{AC}$ is the split flow rate (kg_a/s), and x_{AC} is the mass ratio of the water saturated moist air at the temperature of the air-conditioning system.

The air-conditioning system was modelled in a relatively simple way. As this

work focuses on the impact of the occupancy scenario on the hygrothermal performance of a room, the perturbations induced by the air-conditioning system were deliberately limited. This modelling strategy led to short cycles of ON and OFF states to keep the indoor temperature and relative humidity at the defined set points, which is not representative of a real regulation. Also, the efficiency of the air-conditioning system was not considered in this work. Still, this approach was satisfactory to keep the indoor temperature and relative humidity in the defined ranges to simulate realistic indoor conditions.

4.2 Stochastic occupancy model

4.2.1 Presence model

In this case, the occupants' presence and activities were modelled thanks to Nottingham Multi-Agent Stochastic Simulation (No-MASS) platform [19]. Within No-MASS, the occupants' presence (or absence) in non-residential buildings is modelled in accordance with the model developed in Ref. [13]. This model verifies whether an occupant is present within a zone of the building, under the assumption that the probability of presence at a time step depends only on the state of presence at the previous time step. Mathematically, this statement corresponds to considering the state of occupancy as a Markov chain. As the probability of an occupant arriving or leaving an office is not the same depending on the time of the day, the Markov chain is inhomogeneous. The model inputs are a time-dependent profile of probability of presence and a parameter of mobility characterizing the ability of an occupant to leave the room for a short while. Ref. [37] gives details on how to estimate the state of presence at each time step.

The validation of the model relied on data provided by the monitoring of twenty zones in an office building for five years [13]. No-MASS gives the occupants' presence in an office with a 5 minute time step. This step was chosen after a time step sensitivity study presented in Ref. [38].

4.2.2 Metabolic heat gains and vapor production

The metabolic heat generated by an occupant was calculated in No-MASS in accordance with the standard ISO 7730 [40]. The heat gains depended on the indoor air conditions, namely the air temperature and the relative humidity.

As there is no standard dedicated to the calculation of water vapor production, a constant value of 48 g/h per occupant was chosen, based on Ref. [41].

4.2.3 Heat production due to the occupants' activities

While the metabolic heat gains and vapor production presence were estimated in No-MASS, the heat production due to the occupants' activities was deduced from a literature review and implemented in our model.

For offices, it was assumed that, upon arrival, an occupant turned on a computer and turned it off upon his departure every day, and that a constant heating power of 150 W, based on Ref. [15], was generated. During short absences of the occupant through the day, the computer was kept on. The variation of heat generation depending on the use of the computer (sleep mode, word processing, watching videos, etc.) was not considered.

During the night, the lights were turned on from one hour before sunset to one hour after sunrise if an occupant was present in the room. Lighting produced a constant heat of 10 W/m^2 [39].

4.2.4 Coupling No-MASS with the *Room model*

While the occupants' presence and activities were modelled in No-MASS, the model regrouping the hygrothermal balance on indoor air, the coupled heat and moisture transfer through the walls and the indoor sources due to the air-conditioning system were written in PYTHON. This model is referred to as *Room model*.

The metabolic heat gains depended on the indoor environmental conditions — calculated by the *Room model* — which varied at each time step. No-MASS was

hence coupled with the *Room model*. As No-MASS is written in C++ and the room model in PYTHON, the coupling approach relied on the use of a Functional Mockup Interface (FMI) (Fig. 4).

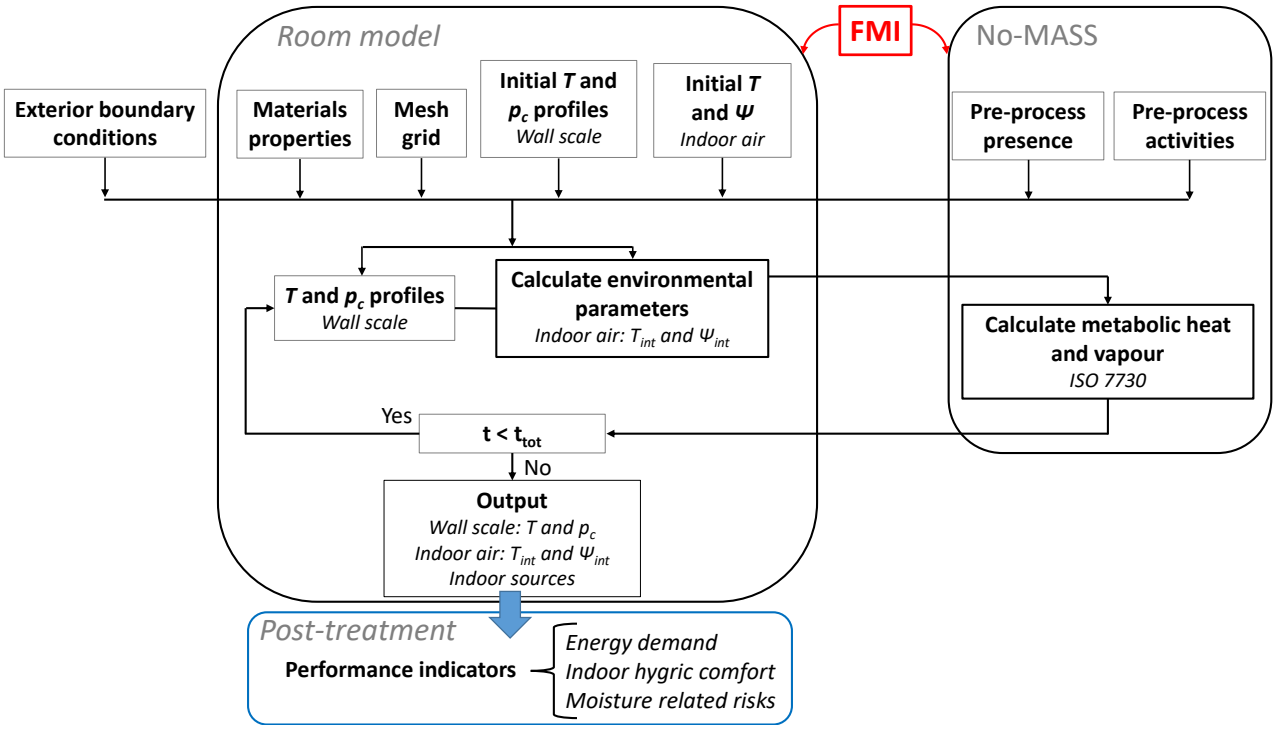


Figure 4: Exchange of data between the Room Model and No-MASS

At the beginning of a simulation, the occupants' presence and activities were pre-processed in No-MASS as they are independent of the indoor environmental parameters (temperature and relative humidity). The initial temperature and capillary pressure profiles in the wall, and the indoor temperature and relative humidity are defined in the *Room model*. At the next time step, these parameters were first calculated by the *Room model* before being communicated to No-MASS. No-MASS then determined the metabolic heat gains and vapor production. The process continued until the end of the simulation.

The simulation results were the temperature and capillary pressure in the walls, the indoor conditions, and the power and vapor production of the air-conditioning system obtained with a time step of 5 minutes. These parameters can be used to compute performance indicators once the simulation is completed. They are defined

in the next section.

5 Definition of performance indicators

5.1 Energy demand

The estimation of the energy demand of a room was straightforward as it corresponded directly to the demands of the air-conditioning system, i.e. the heater, the humidifier and the split air-conditioner.

For the heater, the energy demand was given directly by its power $\dot{Q}_{heat}$.

The humidifier generated water vapor at a constant rate $\dot{m}_{humid}$. Its energy consumption was determined by:

$$\dot{Q}_{humid} = \dot{m}_{humid} \left(c_{p,v} T + L_v \right) \tag{17}$$

where T corresponds to the temperature needed to produce water vapor (100°C).

The air-conditioner power $\dot{Q}_{AC}$ (W) was calculated at each time step using Eq. (18), which is based on a thermodynamic balance.

$$\dot{Q}_{AC} = \dot{m}_{AC}(h_{AC} - h_{int}) \tag{18}$$

where h_{AC} is the specific total enthalpy of the air in the split (J/kg). Note that the efficiency of the system was not included.

5.2 Hygric comfort

The occupants' comfort is a subjective notion that may differ widely from one individual to another. Factors influencing it can be personal (metabolic rate, clothing type, thermal sensitivity, etc.) and environmental (room temperature and relative humidity, air velocity etc.). According to Ref. [42], the most widely used comfort

criterion is the one from the ASHRAE standard 55 [43]. It was developed using surveys carried out on individuals placed in controlled chambers. This led to the definition a comfort zone constrained by threshold values on the temperature (between 19 and 26°C) and the relative humidity (between 30 and 70%)

However, in the case of controlled environmental conditions in a room, the wide range of temperature and relative humidity covered by these intervals might lead to inconsistent results. Consequently, the criterion from Ref. [44] was selected because it is more restrictive. It defines the comfort zone for a relative humidity between 40 and 50%. The air was deemed *comfortable* for a humidity between 40 and 50%, *too dry* under 40% and *too humid* above 50%.

5.3 Moisture related risks

High relative humidity might lead to mould growth on the surface and/or inside the wall assemblies. The proliferation of fungi on a wall can result in the spread of pathogens in the air, which impact the health of the occupants. Within the wall, mould may deteriorate the wall assemblies, directly affecting the hygrothermal and mechanical performance of the structure.

In the literature, different models have been developed to predict mould growth. A brief review can be found in Ref. [45]. In this work, the isopleth model from Ref. [46] was chosen. An isopleth is a graph describing the risk of proliferation of bacteria according to temperature and relative humidity. Temperature and relative humidity pairs for each time are represented on a scatter plot. A hyperbolic limit curve is also plotted, determining the threshold value of temperature and relative humidity pairs for which mould growth could occur. Different equations can be used to determine the limit curve. In Ref. [46] a parabolic equation is used, described by Eq. (19):

$$\Psi = a + c(T^2 - 54T) \tag{19}$$

with Ψ in (%). a and c are given by Eq. (20):

$$\begin{aligned} c &= (\Psi_{crit1} - \Psi_{crit2}) / \left[T_1^2 - T_2^2 - 54(T_1 - T_2)\right] \\ a &= \Psi_{crit1/2} - c(T_1^2 - 54T_1) \end{aligned} \tag{20}$$

where $T_1 = 22°\text{C}$ and $T_2 = 10°\text{C}$ define the range in which a critical moisture level is expected [47]. To determine Ψ_{crit1} and Ψ_{crit2}, Johannson et al. [47] put samples of different materials in humidity-controlled chambers, with humidity set at intervals of 5%. Therefore, two curves were defined corresponding to the humidity for which mould appeared and the next-lowest humidity. To be on the safe side, it was assumed that mould appeared if the temperature and humidity pairs were above the lower curve. As the widest range of materials seem to be covered in Ref. [46], this model was implemented in the *Room model*.

6 Case study

In the aim of estimating the impact of the occupancy scenario on the performance indicators, different occupancy scenarios were applied to the configuration of only one office, of dimensions 5 m × 5 m × 2.5 m. The external wall, made of 20 cm of concrete, 13 cm of gypsum board and 1.3 cm of plaster, was facing south. The office was assumed to be surrounded by other offices where indoor temperature and relative humidity evolved in the same way as in the simulated office. A symmetry condition was hence applied. The separating walls were made of two 1.3 cm thick gypsum boards with 6 cm of polystyrene in between. The floor and ceiling were made of 20 cm of concrete. To simulate a conventional interior coating acting as a vapor barrier, a vapor resistance Sd equal to 0.5 m was added to all the walls. Its thermal properties were considered negligible. No coating was added on the exterior surface. The material properties are given in the Appendix.

Two male occupants were present in this office. Their sole activity, was working

on a computer. The use of lighting and computers were simulated in accordance with the method described in Section 4.2.

The exterior boundary conditions were those found in Trappes (France) as they were considered to be representative of the French climate (temperate climate). They were given by the French regulation [8]. The simulations were run on one year of weather data starting on 1st January, assuming it was a Monday for the occupancy scenario.

The initial conditions were obtained by repeating the simulated year until the relative difference in capillary pressure and temperature fields in the walls between two consecutive years was below 2%. This was obtained after repeating the simulation for 5 years. The initial indoor air temperature and vapor pressure were those obtained after these 5 years.

6.1 Air-conditioning system

First, set point temperatures and relative humidities were selected for the air-conditioning system. For the heater, the set point temperatures was 21°C for the day and 19°C for the night. The set point relative humidity of the humidifier was 40% as this corresponds to the lower boundary of the interval of comfort defined in [44]. It was only turned on during working hours. For air cooling, the set point temperature of the air-conditioner was 24°C. Like the humidifier, it was only turned on during working hours. As the air dehumidification was a consequence of air cooling, no set point relative humidity was defined for it.

The air-conditioning system was sized by means of a mass and energy balance under steady conditions. For the heater and the humidifier, the exterior temperature and relative humidity of reference were -5 °C and 60% respectively [8]. The sizing of the air-conditioner was based on the maximum indoor heat load (two occupants, two computers and lights turned on). This led to the choice of the following power and water vapor production for the air-conditioning system:

- The heater power was 1500 W;
- The humidifier rate was 0.35 kg_v/h;
- The split air flow rate was 0.1 kg_a/s.

6.2 Occupancy scenario

Four occupancy scenarios representative of the most common scenarios found in the literature were simulated: a stochastic scenario, an average one, a constant one and a deterministic one.

6.2.1 Scenario 1: SC1 — No-MASS scenario

No-MASS scenarios were obtained according to the methodology presented in Section 4.2.

A seasonal effect was implemented and was especially pronounced on the lighting energy. This is exemplified by Fig. 5, which presents the total heat generated per month by the occupants and the lighting through a full year.

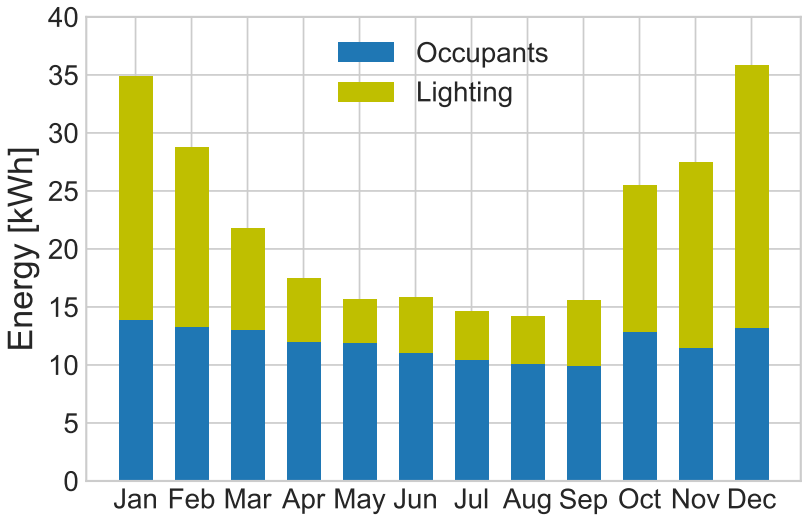


Figure 5: Energy generated by the occupants and the lights over a year

First, the metabolic heat gain was lower in summer than in winter. The average energy generated by the occupants was 40.4 kWh in winter, and 30.5 kWh in summer, corresponding to a difference of approximately 32%. The standard ISO 7730 [40] states that the metabolic heat gain depends on temperature and relative humidity. Therefore, high temperature and relative humidity in summer lead to lower heat gains than in winter.

The energy generated by the lights was approximately 4.2 times greater in winter than in summer, with an average value of 59.0 kWh for the former period and 13.9 kWh for the latter. This was expected, as we considered sunrise and sunset times as well as the occupants' arrival and departure times to model the use of lights.

6.2.2 Scenario 2: SC2 — Average scenario

No-MASS was run independently 850 times from the *Room model* to generate a different occupancy scenario each time. An average scenario was then deduced and repeated every day, except for the weekends. A large number of simulations was chosen because we wanted the scenario to follow a normal distribution. The average metabolic heat gain was then deduced by verifying the following equation at each time t:

$$\dot{Q}^{t}_{occ,SC2} = \frac{\sum_{i=0}^{N} \dot{Q}^{t}_{occ,i}}{N} \tag{21}$$

where $Q^{t}_{occ,SC2}$ and $Q^{t}_{occ,i}$ are the metabolic heat gains from SC2 and the i-th stochastic simulation, respectively, at time t and N corresponds to the number of stochastic simulations (850). As the metabolic heat was integrated over a year, the seasonal effect was not taken into account. The average gain was 68 W for the two occupants. The lighting and the use of computers were implemented in a similar fashion to in SC1.

For the air-conditioning system, the start and stop times were fixed at 7:35 am and 5:25 pm respectively. These values corresponded to the average arrival and

departure times.

6.2.3 Scenario 3: SC3 — Constant scenario

The constant scenario was obtained by integrating the occupants' metabolic heat gains and vapor production, and the power for computers and lighting over one year. The heat gains were obtained from the following equation:

$$\dot{Q}_{SC3} = \frac{1}{t_{max}} \int_0^{t_{max}} \dot{Q}_{SC2} dt \tag{22}$$

where t_{max} corresponds to one year. The seasonal effect was therefore not implemented. This led to a constant heat source of 131 W. Approximately 24% of this power, i.e. 31 W, was attributed to the occupants. The vapor production was 22 g/h. Note that the heat and vapor were continuous every day, even during the weekends.

The start and stop times of the air-conditioning system were the same as in SC2.

6.2.4 Scenario 4: SC4 — French regulation scenario

The deterministic scenario simulated was that from the Th-BCE method proposed in the French regulation [8]. This scenario was significantly different from the other three as the objective was to highlight the differences between the scenarios derived from No-MASS and the one used to size new building constructions in France. The differences with the other scenarios are listed below:

- The occupants were present from 8:00 am to 6:00 pm every day except during the weekends;
- The set point temperatures for the heater were 19°C for the day and 16°C for the night;
- The set point temperatures for the air-conditioner were 26°C for the day and 30°C for the night;

- The lights were turned on continuously from 9:00 am to 6:00 pm (i.e. when the occupant was present);
- No computers were simulated, but a heat load corresponding to the use of electrical devices was added. It was equal to 80 W when the occupant was present.

Note that the set point temperatures for the heater and the air-conditioner were different from the ones initially input to the *Room model*. We believe that the set point temperatures indicated in the RT are not representative of a realistic regulation of offices. Temperatures of 21°C (day) and 19°C (night) for the heater and 24°C (day) for the air-conditioner seem more plausible.

6.2.5 Summary

For illustration purposes, the four different occupancy scenarios are plotted in Fig. 6, with the metabolic heat gains corresponding to two occupants reported on the y-axis. For the stochastic scenario (top left), the graph corresponds to the occupancy profile for a random day and for a single scenario. For SC1-3, the total metabolic gains over the year were the same. This does not mean that the personnel density was the same for each scenario. For SC4, a constant metabolic heat gain of 90 W was selected in accord with the French regulation [8], leading to a different total metabolic gain over the year than the ones from SC1-3. Table 1 lists the indoor sources.

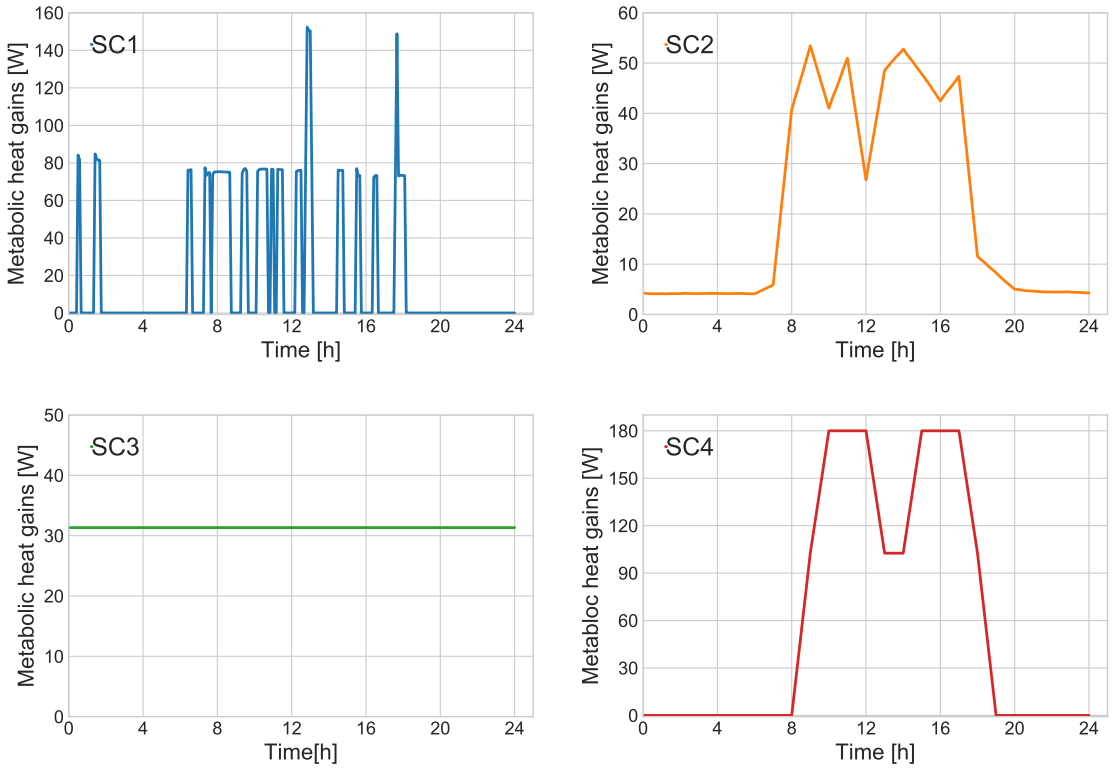


Figure 6: Stochastic (top left), average (top right), constant (bottom left) and deterministic (bottom right) occupancy scenarios

		SC1-3	SC4
Set point *day/night*	Heater	21/19 ± 0.5°C	19/16 ± 0.5°C
	Humidifier	40%/OFF ± 2%	40%/OFF ± 2%
	Air-conditioner	24/OFF ± 0.5°C	26/30 ± 0.5°C
	Electrical devices (W)	300	80
	Lighting (W/m^2)	10 (at night, if occupant)	10 (working hours)
	Metabolic heat (W)	Variable (average: 68)	90
	Metabolic vapor (g/h)	48	60

Table 1: Indoor sources for SC1-4

Note that the metabolic heat gain was never zero for SC2. In No-MASS, the probability of presence at night-time was implemented (though low) because an office worker or the cleaning service, for example, might be working. This can also be seen in SC1 graph, where an occupant was present for a short time between 12:00

am and 3:00 am. Consequently, averaging the vapor production over 850 simulations led to non-zero heat and vapor production during the night.

As Fig. 6 presents only the metabolic heat gains, it does not give any information on the total heat generated by the occupants, the lighting and the computers. Therefore, Fig. 7 provides an example of the total heat gains over a random day for the stochastic scenario.

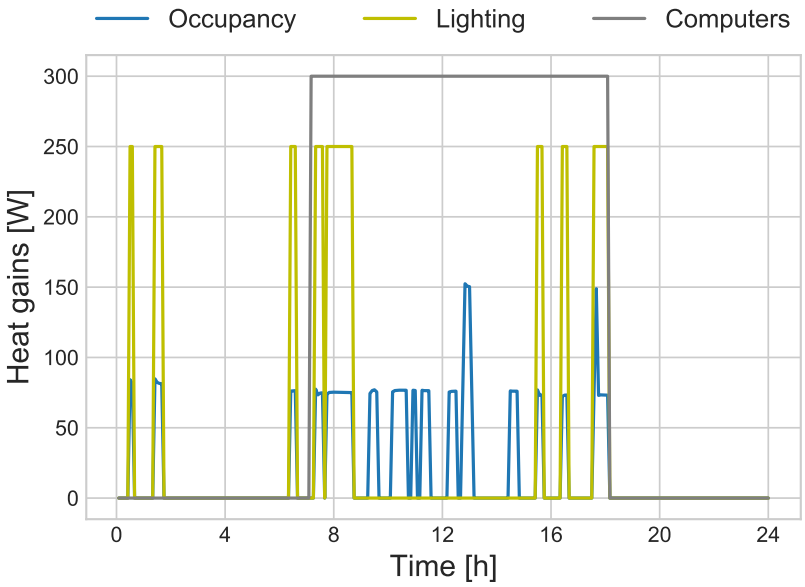


Figure 7: Heat gains over a random day for the stochastic scenario

7 Results and discussion

In order to take the stochastic behaviour of the occupants into consideration, 10 SC1 simulations were run with a different occupancy scenario each time. Results were averaged, and the standard deviation is reported on the figures.

7.1 Energy demand

The energy demand of the room corresponds to that of the air-conditioning system. Its behaviour varied greatly from one day to another because of short cycles

of ON and OFF states. Therefore, results are presented at yearly and monthly scales. Fig. 8 presents the energy consumption integrated over each month for one year. More details are provided in Table 2 for two months representative of typical heating and cooling conditions.

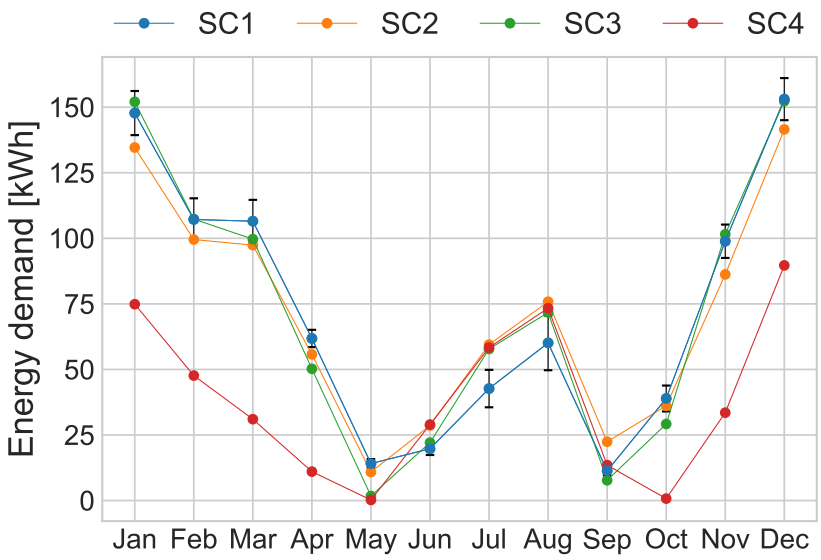


Figure 8: Energy consumption of the equipment for each occupancy scenario

		Energy demand (kWh)		
		Heater	Humidifier	Air-conditioner
SC1	*January*	141 ± 8	7 ± 0.4	—
	August	—	—	60 ± 5
SC2	*January*	128	7	—
	August	—	—	76
SC3	*January*	141	11	—
	August	—	—	72
SC4	*January*	73	2	—
	August	—	—	73

Table 2: Energy demand in January and in August for SC1-4

First, high energy demands were obtained in January (128 kWh for SC2 for example) and in August (76 kWh for SC2) due to heating and cooling needs re-

spectively. Most of the energy demand was for heating purposes in January as the humidifier represented between 2 and 8% of the total energy demand during this month for SC1-3. Only the air-conditioner was turned on in summer.

A lower (approximately 10%) energy demand is observed for SC2 compared to SC1 in January, but it is higher in August (around +32%) for SC2. While SC2 was derived from multiple SC1 scenarios, the energy demand observed for SC2 is often beyond SC1 dispersion. The air-conditioning system, the use of the computers and the use of the lights were modelled in the same way for SC1 and SC2, but the latter did not take the seasonal effect into account as the same occupancy scenario was repeated every day. Moreover, SC2 metabolic heat gain was set constant and equal to 68 W. For SC1, it was lower in summer than in winter as it varied with the air temperature and relative humidity (see Fig. 5). Therefore, the cooling demand for SC2 was higher than that for SC1 in summer. The same trend was observed between SC1 and SC3.

For SC4, because the set point temperatures were set to lower values than in the other scenarios, energy demand was expected to be lower in January and higher in August. SC4 underestimated the yearly energy demand by 84% compared to SC1. Chapman et al. [19] compared a deterministic scenario (implemented in DesignBuilder software [48]) and No-MASS stochastic scenario for an office located in Nottingham and another in Geneva. They showed an underestimation of approximately 20% of the energy demand with the deterministic scenario. This comparison was similar to the one between SC1 and SC4 in our case.

The yearly energy demand is summarized in Table 3 in which the latent contribution of the air-conditioner corresponds to the amount of air dehumidified.

	Energy demand (kWh)				
	Heater	Humidifier	Air-conditioner		Total
			sensible	*latent*	
SC1	690 ± 25	44 ± 1.4	80 ± 7	47 ± 4	851 ± 37
SC2	640	30	116	64	850
SC3	645	52	99	58	854
SC4	282	9	110	62	463

Table 3: Yearly energy demand for SC1-4

While SC2 and SC3 heating demands were within SC1 dispersion in January, this is not the case at the yearly scale because of a higher dispersion recorded for the other cold months.

SC2 led to 8% less heating demand, 47% less humidifying demand, but 36% more cooling demand than the average demand of SC1. The same trend is observed for the heating and cooling needs of SC3 as it led to 8% less heating demand and 32% more cooling demand than SC1. The humidifying demand was, however, 18% higher. These results are consistent with the seasonal effect as SC2 and SC3 required more heating in winter and less cooling in summer than SC1. The higher humidifying demand for SC3 is discussed in the next section.

7.2 Hygric comfort

Fig. 9 shows the indoor relative humidity distribution over one year for each scenario in 2% humidity intervals, where the abscissa represents the mean value of each interval (for example the abscissa 41 corresponds to the interval [40;42]%). Only the humidity recorded during working hours is presented in this figure. The time spent in the comfort zone for each scenario is summarized in Table 4.

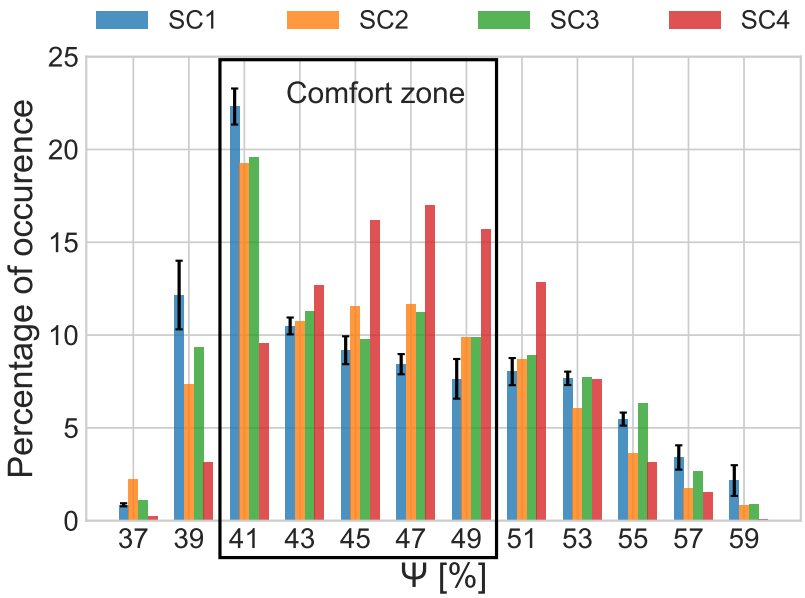


Figure 9: Indoor relative humidity distribution over a year for each occupancy scenario

	Comfort zone [40;50]%
SC1	58.1 ± 1.9%
SC2	68.4%
SC3	62.7%
SC4	71.4%

Table 4: Time spent in the comfort zone for SC1-4

Overall, SC1 led to a smaller amount of time spent in the comfort zone than SC2-4. Note that few deviations on the time spent in the comfort zone are observed between the different SC1 scenarios.

First, a comparison was made between SC1 and SC2. The humidifier energy demand was higher for SC1 than for SC2 (see Table 3), and it was turned on for an average of 104 days during the year against 91 days for SC2. The air was thus drier for SC1. Moreover, a seasonal effect was noticed on occupancy. As the occupants generated less heat in summer for SC1 than for SC2, the indoor load was more significant for SC2. It engendered a higher cooling need and air dehumidification. This is noted in Table 3, with a 36% higher latent energy demand. Comparing

the two scenarios in summer, SC2 led to around 10% more time being spent in the comfort zone than SC1. The comfort prediction of SC2 is beyond to SC1 dispersion, indicating a non-negligible impact of the occupancy scenario.

We now compare SC3 and SC1. While the energy demand of the humidifier was 16% higher for SC3 than for SC1, it led to a higher prediction of the comfort range. As SC3 smoothed the metabolic vapor production, the seasonal effect on occupancy was not taken into account. Consequently, the indoor vapor load of SC3 was smaller than that of SC1 in winter, requiring more use of the humidifier. This is also reflected by the fact that the humidifier was turned on for 127 days in SC3 against an average of 104 for SC1. Finally, as for SC2, the seasonal effect on occupancy also led to 7% more time being spent in the comfort zone than for SC1 in summer.

SC4 led to a higher overall indoor relative humidity than SC1-3. This can be explained by two factors. Firstly, the set point temperatures for SC4 were lower than for SC1-3 in winter. For the same amount of water vapor produced, a lower temperature led to a higher relative humidity. Secondly, more vapor was generated by the occupants (60 g/h per occupant against 48 g/h for SC1-3). This led to 71.4% of the time being spent in the comfort zone.

Labat and Woloszyn [21] compared a stochastic scenario to a constant one in a simulated dwelling where one occupant was living. They observed that using a constant moisture production scenario could lead to an increase of 10 to 20% of the comfort range (using the same comfort criterion as in Ref. [44]). While not of the same order of magnitude, this trend was also observed here between SC1 and SC3, as SC3 led to an increase of approximately 4.6% of the comfort range. In Ref. [21], due to the occupant's various activities (cooking, showering, use of washing machine, etc.) the water vapor production was not only metabolic, which led to an average moisture production of 82 g/h over one year. The average vapor production for the stochastic scenario in our simulated office was 22 g/h, which is approximately 3.7 times lower. This could explain the difference in indoor comfort between the case

study in Ref. [21] and ours.

7.3 Moisture related risks

Two isopleths were plotted for each scenario. The first one was at the interior surface of the exterior wall, because if mould growth were to appear, it could impact the health of the occupants. The other one was at the interface between the insulation material (polystyrene) and the concrete because humidity is more prone to accumulate there, which could lead to thermal and/or structural issues.

The plaster limit curves were calculated in accordance with Eq. (19). The critical relative humidity was 89% for the lowest curve and 95% for the highest. For the polystyrene, it was assumed that mould growth would appear only for a relative humidity above 95% [46].

The results are presented in Figs. 10 and 11. For the sake of clarity, SC4 was plotted separately from SC1-3. Note that only the results for a single SC1 scenario are plotted in this figure as few discrepancies were observed between the scenarios. The limit curves were plotted in black on these figures.

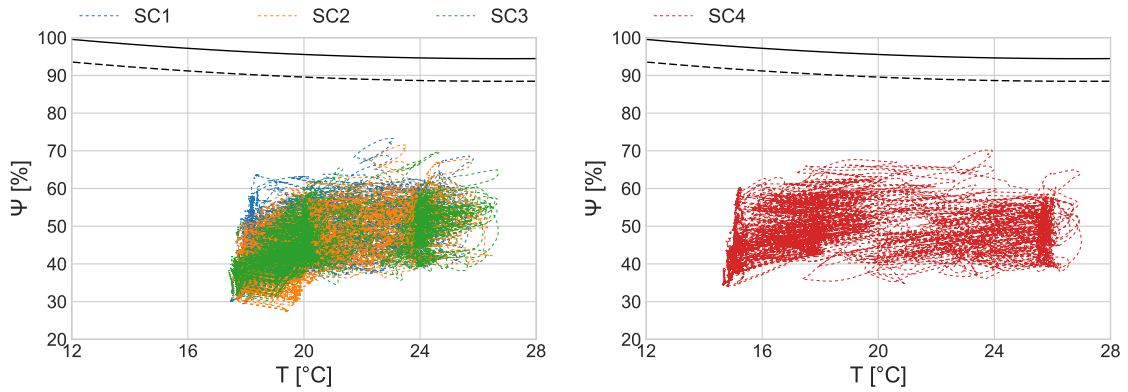


Figure 10: Isopleth at the surface of the exterior wall for SC1-3 (left) and SC4 (right)

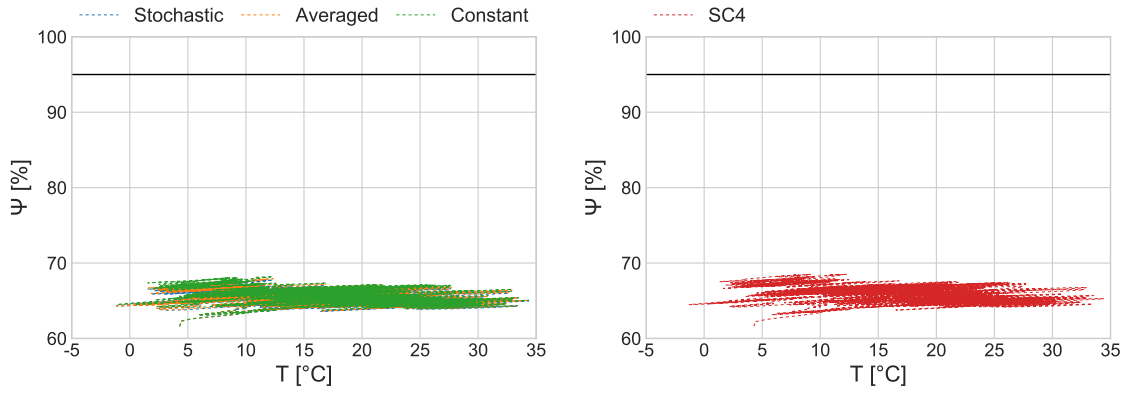


Figure 11: Isopleth at the interface between the polystyrene and the concrete for SC1-3 (left) and SC4 (right)

All the scatter plots are well below the limit curves, meaning that there is no risk of mould growth for any scenario. Additionally, SC1-3 isopleths at the surface of the wall and also at the interface between the polystyrene and the concrete are very close to each other. Note that, because of these small deviations, SC1 plot is masked by SC2-3 in Fig. 11. Fig. 10 also confirms the results in Fig. 9 which presents a similar humidity distribution for SC1-3. For SC4, the larger spread of the isopleth at the surface is due to the different set point temperature defined.

At the interface between the polystyrene and the concrete, the temperature is spread from -1°C to 33°C. Because of the high thermal conductivity of concrete (2 $W/(m.K)$), this zone was largely influenced by the exterior environmental conditions. This also explained why SC4 gave similar results to those of SC1-3. The humidity did not vary much since concrete has a low vapor permeability; most of the vapor flux was compensated by the first centimetres of the material.

8 Conclusion and perspectives

This article has proposed a methodology for estimating the influence of the occupancy scenario on the hygrothermal performance of a room. To do this, four scenarios representative of the modelling approaches available in the literature were simulated: a stochastic occupancy scenario, an average one (similar to a deter-

ministic scenario), a constant one and, additionally, the French regulation scenario extracted from RT 2012 [8]. The hygrothermal performance of the room was defined by the three performance indicators: the energy demand, the indoor hygric comfort and the moisture related risks.

Discrepancies were observed on the energy demand of each air-conditioning equipment from one scenario to another. They could reach as much as 36% of difference, highlighting a significant impact of the occupancy scenario.

On the indoor hygric comfort, the constant scenario and the average one led to an overestimation of the comfort range by approximately 10.3% and 4.6% respectively compared to the stochastic scenario. These differences were explained by a seasonal effect on occupancy engendering a different regulation on the air-conditioning system.

The French regulation [8] scenario was considered to be separate from the other three because the set point temperature and the simulation of equipment were different. Still, it gave a comparison with the regulation governing new building constructions in France. It led to an underestimation of the energy demand by approximately 84% and a overestimation of the hygric comfort prediction by 13% for this specific case.

No moisture related risks were observed, but the climate of Trappes is temperate. The indoor relative humidity was almost always lower than 70% throughout the year.

To conclude, the impact of the occupancy scenario on the performance indicators (except for the moisture related risks) is strongly dependent on the scale at which we analyse the results. At yearly scale, its influence on the energy demand was negligible and the indoor hygric comfort was significantly impacted. However, at seasonal scale, the impact was more pronounced: the seasonal effect on occupancy was smoothed by the deterministic and constant scenarios compared to the stochastic one. For example, there were differences between the occupancy scenarios of up to 36% on the cooling demand and up to 10.3% on the time spent in the comfort

zone in summer.

This methodology shows significant discrepancies between the different scenarios. The importance of using calibrated and validated stochastic occupancy models in the aim of simulating indoor hygrothermal conditions was highlighted. This work will be extended to other case studies, in particular by simulating indoor plasters in order to investigate their influence.

9 Acknowledgements

This work benefited from the valuable contribution of Pr. Darren Robinson and Dr. Jacob Chapman of the University of Sheffield — School of Architecture (England), who kindly provided the No-MASS platform used in this work.

References

[1] R. Diasty, P. Fazio, and I. Budaiwi. Modelling of indoor air humidity: the dynamic behaviour within the enclosure. *Energy and Buildings*, 19:61–73, 1992.

[2] C. R. Pedersen. *Combined Heat and Moisture Transfer in Building Constructions*. PhD thesis, Technical University of Denmark, Denmark, 1990.

[3] H. M. Künzel. *Simultaneous Heat and Moisture Transport in Building Components - One- and two-dimensional calculation using simple parameters*. PhD thesis, Fraunhofer Institute of Building Physics, Stuggart, Germany, 1995.

[4] J. Delgado, E. Barreira, N. Ramos, and V. de Freitas. A critical review of hygrothermal models used in porous building materials. *Journal of Porous Media*, 13(3):231–234, 2010.

[5] M. Woloszyn and C. Rode. Tools for performance simulation of heat, air and moisture conditions of whole buildings. *Building Simulation*, 1(1):5–24, March 2008.

[6] N. Hutcheon. Humidity in Canadian buildings. In *Canadian Chapters Conference*, Toronto, Canada, 1955.

[7] I. S. Walker and M. H. Sherman. Humidity implications for meeting residential ventilation requirements. In *Lawrence Berkley National Laboratory*, Berkley, California, 2007.

[8] RT Bâtiment. RT neuf 2012: Données météorologiques, 2012. `http://www.rt-batiment.fr/batiments-neufs/reglementation-thermique-2012/donnees-meteorologiques.html`, accessed 6.14.17.

[9] M. Qin, G. Walton, R. Belarbi, and F. Allard. Simulation of whole building coupled hygrothermal-airflow transfer in different climates. *Energy and Conversion Management*, 52:1470–1478, 2011.

[10] H. Künzel, A. Holm, D. Zirkelbach, and A. Karagiozis. Simulation of indoor temperature and humidity conditions including hygrothermal interactions with the building envelope. *Energy and Buildings*, 78:554–561, 2005.

[11] M. Woloszyn, T. Kalamees, M. Olivier Abadie, M. Steeman, and A. Sasic Kalagasidis. The effect of combining a relative-humidity-sensitive ventilation system with the moisture-buffering capacity of materials on indoor climate and energy efficiency of buildings. *Building and Environment*, 44(3):515–524, March 2009.

[12] S. Hameury. Moisture buffering capacity of heavy timber structures directly exposed to an indoor climate: a numerical study. *Building and Environment*, 40:1400–1412, October 2005.

[13] J. Page, D. Robinson, N. Morel, and J.-L. Scartezzini. A generalised stochastic model for the simulation of occupant presence. *Building and Environment*, 40:83–98, 2008.

[14] Q. Darakdjian, S. Bille, and C. Inard. Data mining of building performance simulations comprising occupant behaviour modelling. *Advances in Building Energy Research*, 139:214–223, 2017.

[15] S. Jaboob. *Stochastic modelling of occupants' activities and related behaviours*. PhD thesis, University of Nottingham, Nottingham, 2015.

[16] F. Haldi and D. Robinson. Interactions with window openings by office occupants. *Building and Environment*, 44(12):2378–2395, 2009.

[17] F. Haldi and D. Robinson. Adaptative actions on shading devices in response to local visual stimuli. *Journal of Building Performance Simulation*, 3(2):135–153, 2009.

[18] C. Reinhart. Lightswitch-2002: a model for manual and automated control of electric lighting and blinds. *Solar Energy*, 77(1):15–28, 2004.

[19] J. Chapman, P.-O. Siebers, and D. Robinson. On the multi-agent stochastic simulation of occupants in buildings. *Journal of Building Performance Simulation*, 11(5):604–621, 2018.

[20] A. Cowie, T. Hong, X. Feng, and Q. Darakdjian. Usefulness of the obFMU module examined through a review of occupant modelling functionality in building performance simulation programs. In *IBPSA Building Simulation*, San Francisco, USA, 2017.

[21] M. Labat and M. Woloszyn. Moisture balance assessment at room scale for four cases based on numerical simulations of heat-air-moisture transfers for a realistic occupancy scenario. *Journal of Building Performance Simulation*, 9(5):487–509, November 2015.

[22] R. Bui, M. Labat, and S. Lorente. Impact of heat and moisture transfer through a multilayer wall on the comfort conditions of an occupied room. In *15th Canadian Conference on Building Science and Technology*, Vancouver, Canada, 2017.

[23] J. Winkler, J. Munk, and J. Woods. Effect of occupant behavior and air-conditioner controls on humidity in typical and high-efficiency homes. *Energy and Buildings*, 165:364–378, 2018.

[24] B. Seng, S. Lorente, and C. Magniont. Scale analysis of heat and moisture transfer through bio-based materials - application to hemp concrete. *Energy and Buildings*, 155:546–558, 2017.

[25] S. Lorente. The constructal law as an approach to address energy efficiency in the urban fabric. In *Constructal Law And Second Law Conference*, Bucharest, Romania, 2017.

[26] F. Tariku, K. Kumaran, and P. Fazio. Transient model for coupled heat, air and moisture transfer through multilayered porous media. *International Journal of Heat and Mass Transfer*, 53(15-16):3035–3044, July 2010.

[27] A. S. Kalagasidis, C. Rode, and M. Woloszyn. HAM-Tools: a whole building simulation tool in annex 41. *IEA EACBS Annex 41*, 130:21–35, 2008.

[28] A. van Schijndel. Multiphysics modeling of building physical constructions. *Building Simulations*, 4(1):49–60, 2011.

[29] A. Bejan. *Convection Heat Transfer*. Wiley & Sons, Hoboken, 4 edition, 2013.

[30] S. V. Patankar and B. R. Baliga. A New Finite-Difference Scheme for Parabolic Differential Equations. *Numerical Heat Transfer Part B - Fundamentals*, 1:27–37, January 1978.

[31] S. V. Patankar. *Numerical Heat Transfer and Fluid Flow*. Hemisphere Publishing Corporation, 1980.

[32] G. van Rossum. Python tutorial, technical report CS-R9526. In *Centrum voor Wiskunde en Informatica (CWI)*, Amsterdam, 1995.

[33] G. Soderlind and L. Wang. Adaptive time-stepping and computational stability. *Journal of Computational Methods in Sciences and Engineering*, 2(3):1–3, 2003.

[34] Afnor. EN 15026 - Hygrothermal performance of building components and building elements - Assessment of moisture transfer by numerical simulation. 2007.

[35] H. Janssen, B. Blocken, and J. Carmeliet. Conservative modelling of the moisture and heat transfer in building components under atmospheric excitation. *International Journal of Heat and Mass Transfer*, 50(5-6):1128–1140, March 2007.

[36] Arrêté du 24 Mars 1982. http://www.legifrance.gouv.fr/affichtexte.do? cidtexte=jorftext000000862344. 1982.

[37] J. Page. *Simulating occupant presence and behaviour in buildings*. PhD thesis, Ecole Polytechnique de Lausanne, Switzerland, 2007.

[38] J. Chapman, P.-O. Siebers, and D. Robinson. Multi-agent stochastic simulation of occupants for building simulation. In *15th IBPSA Conference*, San Francisco, USA, 2017.

[39] H.-J. Steeman, M. Van Belleghem, A. Janssens, and M. De Paepe. Coupled simulation of heat and moisture transport in air and porous materials for the assessment of moisture related damage. *Building and Environment*, 44(10):2176–2184, October 2009.

[40] Afnor. EN ISO 7730 - Ergonomics of the thermal environment - Analytical determination and interpretation of thermal comfort using calculation of the PMV and PPD indices and local thermal comfort criteria. 2005.

[41] P. Johansson, S. Pallin, and M. Shahriari. Risk assessment model applied on building physics: Statistical data acquisition and stochastic modeling of indoor moisture supply in Swedish multi-family dwellings. *In IEA Annex 55 RAP-RETRO. Copenhagen*, 2010.

[42] H. Sulaiman and F. Olsina. Comfort reliability evaluation of building designs by stochastic hygrothermal simulation. *Renewable and Sustainable Energy Reviews*, 40:171–184, 2014.

[43] ASHRAE. Fundamentals thermodynamics properties of water at saturation. atlanta, GA: American society of heating, refrigerating and air-conditioning engineers, inc. 2005.

[44] P. Wolkoff and K. K. Soren. The dichotomy of relative humidity on indoor air quality. *Environment International*, 33(6):850–857, 2007.

[45] E. Vereecken and S. Roels. Review of mould prediction models and their influence on mould risk evaluation. *Building and Environment*, 51:296–310, 2012.

[46] P. Johansson, T. Svensson, and A. Ekstrand-Tobin. Validation of critical moisture conditions for mould growth on building materials. *Building and Environment*, 62:201–209, 2013.

[47] P. Johansson, A. Ekstrand-Tobin, and G. Bok. An innovative test method for evaluation the critical moisture level for mould growth on building materials. *Building and Environment*, 81:404–409, 2014.

[48] DesignBuilder. DesignBuilder software limited, 2014.

[49] H. Künzel, A. Holm, and M. Krus. Hygrothermal properties and behaviour of concrete. *WTA-Almanach*, pages 161–181, 2008.

[50] M. Labat, C. Magniont, O. Nicolaas, and J.-E. Auberty. From the experimental characterization of the hygrothermal properties of straw-clay mixtures to the numerical assessment of their buffering potential. *Building and Environment*, 97:69–81, 2016.

[51] J. Delgado, E. Barreira, N. Ramos, and V. de Freitas. *Hygrothermal Numerical Simulation Tools Applied to Building Physics*. Springer, 2013.

[52] P. Claisse, H. El-Sayad, and E. Ganjian. Water vapour and liquid permeability measurements in mortar samples. *Advances in Cement Research*, 21(2):83–89, 2009.

[53] A. Evrard. *Transient hygrothermal behaviour of lime-hemp materials*. PhD thesis, Université Catholique de Louvain, Louvain, Belgium, 2008.

10 Appendix

	ρ (kg/m^3)	k $(W/(m.K))$	c_p $(J/(kg.K)))$	$\delta_v \cdot 10^{-11}$ (s) dry cup	$\delta_v \cdot 10^{-11}$ (s)	$\delta_v \cdot 10^{-11}$ (s) wet cup
Concrete [49]	2300	1.6	850		0.11 *	
Polystyrene [50]	50	0.04	1450		0.32 *	
Gypsum board [51]	850	0.32	1000	2.6		3.5

Table 5: Material properties extracted from the literature

Concrete [49]	Ψ (%)	20	40	60	80	95	97
	w (kg/m^3)	24.5	34.1	40.4	64.6	108.6	126.1
Polystyrene [50]	Ψ (%)	20	40	60	80	95	97
	w (kg/m^3) $\cdot 10^{-2}$	1.3	1.8	2.6	5.2	20.3	32.9
Gypsum board [51]	Ψ (%)	20	40	60	80	95	97
	w (kg/m^3)	1.5	2.2	3.2	4.4	5.5	6.7

Table 6: Sorption properties

Concrete [52]	$\delta_l(s)$	10^{-17}		
Polystyrene **	w (kg/m^3) $\cdot 10^{-2}$	2.6	5.2	32.9
	δ_l (s)	10^{-17}	10^{-15}	10^{-14}
Gypsum board **	w (kg/m^3)	3.2	4.4	6.7
	δ_l (s)	10^{-17}	10^{-15}	10^{-14}

Table 7: Liquid water permeability

* single value given

** assumption: values corresponding to hemp concrete liquid permeability from [53]